Channels and Melting in Deformable Porous Media

S.L. Butler
Department of Geological Sciences, University of Saskatchewan
146 Science Place, Saskatoon, Saskatchewan, Canada, S7N 5E2, sam.butler@usask.ca

Abstract

Partial melting occurs beneath mid-ocean ridges in Earth's mantle and the resulting liquid migrates to the surface to form new oceanic crust. In this system, mass can be exchanged between the liquid and solid phases through melting and solidification and, at the high temperatures and pressures associated with the Earth's interior, the solid matrix deforms through the process of compaction which may have a significant effect on the transport of the liquid phase. In this contribution, we present a 2D COMSOL model incorporating the effects of compaction and melting and we address the geologically-important issue of the formation and stability of melt channels beneath mid-ocean ridges.

1 Introduction

Melt percolating through a solid porous layer is an important process in a number of geological settings (*Phillips*, 1991). In some situations, such as in melting of the uppermost mantle and in magma chambers (*Shirley*, 1986), the solid matrix may itself deform and flow though viscous creep processes (*McKenzie*, 1984). In such situations, the deformation of the solid matrix may significantly affect the flow of liquid through its interstices. *McKenzie* (1984) presented the equations necessary to model porous flow through compacting media. The fluid and solid matrix are modeled as two interpenetrating fluids with viscosities that differ by orders of magnitude.

Pressure-release melting occurs in the uppermost 30-km of the Earth's mantle beneath mid-ocean ridges and the melt percolates to the surface to form new oceanic crust. Geological evidence suggests that the melt is transported rapidly, likely through high permeability conduits or channels (*Aharanov et al.*, 1995). *Spiegelman et al.* (2001) showed that such channels could be produced by dissolution if the saturation concentration of a solute is a decreasing function of pressure. The compaction of the surrounding porous layer should eventually destroy the high permeability channels, however.

In what follows we will first describe a 2D model, implemented in COMSOL, for the transport of a fluid in a compacting porous layer. In section 3 we use the model to examine the longevity of a pre-existing channel in the presence of compaction effects while in section 4 we couple the model with a heat-transport equation to see if pressure-release melting can cause the spontaneous formation of channels.

2 Governing Equations

We begin with the "classic" compaction equations introduced by McKenzie (1984). These consists of force balance equations for the fluid and solid phases (equations (A20) and (A21) in McKenzie (1984)). The equation governing the velocity of the liquid phase relative to the solid matrix can be written using Darcy's law

$$\mathbf{v} - \mathbf{V} = -\frac{\mathbf{k}_\phi}{\mu\phi}\nabla\mathbf{P}. \qquad (1)$$

Here, $\mathbf{v}$ is the pore velocity of the fluid phase while $\mathbf{V}$ is the velocity of the matrix, P is the non-hydrostatic pressure and ϕ is porosity. The variables k_ϕ and μ represent the permeability of the porous network, and

the viscosity of the fluid phase.

The force balance equation for the solid phase can be written using tensor notation as

$$\frac{\partial}{\partial x_j}[(\zeta^x - 2/3\eta^x)\frac{\partial V_k}{\partial x_k}(1-\phi)\delta_{ij} + \eta^x(1-\phi)(\frac{\partial V_i}{\partial x_j} + \frac{\partial V_j}{\partial x_i})]$$

$$-\frac{\partial P}{\partial x_i} = (1-\phi)(\rho_s - \rho_f)g\delta_{i3}. \quad (2)$$

Here ρ_s and ρ_l are the densities of the solid and liquid phases, ζ^x and η^x represent the bulk and shear viscosities of the matrix, and g represents the acceleration due to gravity. Conservation of mass for the fluid and solid allows us to write the following equations

$$\rho_l[\frac{\partial \phi}{\partial t} + \nabla \cdot (\phi \mathbf{u})] = M, \quad (3)$$

and

$$\nabla \cdot [\phi \mathbf{u} + (1-\phi)\mathbf{U}] = M\frac{(\rho_s - \rho_l)}{\rho_s \rho_l}, \quad (4)$$

where M is the rate of melting or change of mass from the solid to the liquid phase with units $\frac{kg}{m^3 s}$. The permeability, k_ϕ, is given by the following relationship

$$k_\phi = k(x,y)(\frac{\phi}{\phi_0})^n, \quad (5)$$

where $k(x,y)$ is a prescribed function of position used to vary the background permeability while n is taken to have a value of 3 (*McKenzie*, 1984).

These equations and appropriate boundary conditions form a closed system for the velocity of the fluid and matrix as well as the pressure and porosity when M is a prescribed function. We also consider a case when melting is a function of an evolving temperature field. Melting is assumed to occur when the temperature of the fluid exceeds a melting temperature that is a prescribed function of height, T_m, while D is a constant that depends on the melting rates. As such, we calculate melting from

$$M = D(T - T_m). \quad (6)$$

The equations were nondimensionalized using scales for length, velocity, pressure and density of $\delta_c = (k_{\phi_0}\frac{(1-\phi_0)(\zeta^x + 4/3\eta^x)}{\mu_0}))^{1/2}$, $\frac{k_{\phi_0}\Delta\rho g}{\mu_0}$, $\Delta\rho g(\frac{k_{\phi_0}(\zeta^x + 4/3\eta^x)}{\mu_0})^{1/2}$, and ρ_s. Here, ϕ_0 is a reference porosity and the length scale, δ_c, represents the compaction length at the initial porosity. In deformable media, deformation over length-scales much greater than the compaction length is easily accommodated while over length scales much less than the compaction length it is not.

The equations can be written using dimensionless variables that are given the same names as their dimensional counterparts, in a form appropriate for use in the COMSOL time-dependent, general equation formula. The flux vector, Γ, is

$$\begin{pmatrix} -P & 0 \\ 0 & -P \\ -P + \phi'(\frac{\partial U}{\partial x} + \lambda''\frac{\partial V}{\partial y}) & \eta'\phi'(\frac{\partial U}{\partial y} + \frac{\partial V}{\partial x}) \\ \eta'\phi'(\frac{\partial U}{\partial y} + \frac{\partial V}{\partial x}) & -P + \phi'(\frac{\partial V}{\partial y} + \lambda''\frac{\partial U}{\partial x}) \\ (1-\phi)U + \phi u & (1-\phi)V + \phi v \\ \phi u & \phi v \\ 0 & 0 \end{pmatrix} \quad (7)$$

Here $\lambda'' = \frac{\zeta^x - 2/3\eta^x}{\zeta^x + 4/3\eta^x}$, $\eta' = \frac{\eta^x}{\zeta^x + 4/3\eta^x}$ and $\phi' = \frac{(1-\phi)}{(1-\phi_0)}$. The source vector, F, is

$$\begin{pmatrix} \frac{\phi}{k_\phi}(u-U) \\ \frac{\phi}{k_\phi}(v-V) \\ 0 \\ (1-\phi) \\ -M\frac{(1-\rho_l)}{\rho_l} \\ M \\ M - D(T - T_m) \end{pmatrix} \quad (8)$$

The matrix d_a has a single non-zero element in the $(6,6)$ position and has value ρ_l.

An energy equation is used to update the temperature and is entered using the COMSOL heat-transfer transient convection-conduction application mode and is coupled to the other equations using the multiphysics capabilities of COMSOL. The nondimensional energy equation takes the following form:

$$\overline{\rho C_p}\frac{\partial T}{\partial t} + [(1-\phi)\mathbf{U} + \phi\rho_l C_{pl}\mathbf{u}]\cdot\nabla T = \frac{1}{Pe}\nabla\overline{k}\nabla T - MS. \quad (9)$$

Here the nondimensional effective heat capacity is $\overline{\rho C_p} = (1-\phi) + \phi\rho_l C_{pl}$ and we have the nondimensional parameters Pe and S which are a Peclet

number measuring the ratio of advective to diffusive transport over the compaction length and a Stefan number measuring the relative importance of the change in energy due to phase and temperature variations, respectively.

2.1 Dimensionless parameters

The parameters λ'' and η'' characterize the relative magnitudes of the bulk and shear viscosities of the matrix and are given fixed values of 1/7 and 3/7 which are typical for geological materials [*Richter and Daly*, 1989]. The reference porosity, ϕ_0, has a value of 0.01 which is typical of the upper mantle. Melting is fast compared with advection while advection is fast compared with diffusion so D and Pe are given values of 50 and 10 respectively. The Stefan number, S, is given a value of 2. The parameters ρ_l and c_{pl} are the ratios of liquid to solid densities and heat capacities and are given the values of 0.833 and 2, respectively.

2.2 Boundary Conditions

The two side boundaries were taken to have reflection symmetry. At the bottom boundary, fluid was introduced at the fluidization velocity at the reference permeability and porosity, $v = \frac{(1-\phi_0)^2}{\phi_0}$, while the solid matrix was given velocity $V = -(1-\phi_0)$. At the top boundary, the nonhydrostatic pressure and normal stress for the solid matrix were set to 0. For calculations where the energy equation was solved, the temperature was fixed at 1 at the bottom boundary and an outlet flux boundary condition was used at the top.

3 Results 1, Channels with no melting

In the first set of calculations, channels were introduced in which the permeability was increased by a factor of ten over that in the rest of the domain and $M = 0$. The high permeability channels were either the result of using a spatially varying k with constant initial ϕ or varying ϕ with constant initial k. In the absence of a high permeability channel, no compaction will occur because the velocity at which the fluid is injected at the bottom imparts an upward vertical stress on the matrix that is just sufficient to balance the downward force arising from the difference in density between the liquid and solid. The high permeability channel is bounded on the right at $x = 0.5$ and at the top and bottom by $y = 0.5$ and 1.5.

In figure 1a, we show the permeability field at a very early time overlain by an arrow plot for the fluid velocity for a calculation with a constant initial porosity but spatially varying k_ϕ. The initial position of the channel is also shown by the white box as it is in all figures of this type. It can be seen that the fluid is diverted into the channel. It can also be seen that the permeability has evolved due to the effects of compaction. The permeability near the base of the channel has decreased while near the top, it has increased somewhat. In figure 1b, we show the porosity field at the same time as well as an arrow plot for the solid matrix velocity. It can be seen that the porosity is no longer constant and has increased from its initial value of 0.01 near the top of the channel but has strongly decreased throughout most of the rest of the channel. Compaction occurs when fluid flows from a region of low permeability to high permeability such as near the base of the channel. This occurs because fluid is carried away very efficiently and the solid matrix must compact in order to fill the resulting space. When fluid is flowing from a region of high permeability to low permeability, such as at the top of the channel, fluid builds up resulting in decompaction and a resulting increase in porosity and permeability. Because the effects of compaction result in low permeability regions below previous high permeability regions and vice-versa, the permeability field is subject to wave-like phenomena (*Spiegelman*, 1993) with alternating regions of low and high permeability. This wave-like nature can be seen in figures 2a and 2b where we plot the permeability and porosity fields at a dimensionless time of 0.07 along with arrow plots for the fluid velocity (figure 2a) and solid velocity (figure 2b). The high permeability region within the channel near y=1 occurs because of the low permeability region that was formed below

the high permeability region at the top of the initial channel. Similarly, there is now a high permeability region just below the low permeability region that occurs at the base of the initial channel. It can also be seen that much of the fluid flow is now being diverted around the original channel by the low permeability region that develops around the base and lower side of the channel. At this point, almost equal quantities of fluid are flowing inside and outside the channel. It can also be seen that the mean porosity has decreased significantly inside the channel and the system is evolving towards a state where the permeability is roughly the same inside and outside the channel. Over time, the fluid flow was seen to oscillate between being dominantly on the right and left sides of the simulation domain.

The channel is effectively finished by time 0.07, which, when scaled to the Earth's mantle, corresponds to a time of between one month and 2000 years (there are large uncertainties in the compaction length and fluid velocity in the mantle). Even the upper bound on these times is geolgically short and these calculations imply that once channels are formed in the mantle, they will cause complicated flow patterns over relatively short time scales. The initial channels shown have a width of 1 compaction length, corresponding to between 100 and 1000 m. Simulations with significantly narrower channels were also undertaken which were shown to be longer-lived because the matrix will not compact as much over very small length scales. However, even in these calculations the channel broke down over geologically short times. Similar behaviour was also seen when the initial permeability was greater in the channel because of higher porosity.

4 Results 2, Temperature Induced Melting

For these calculations, we introduce a melting temperature that is a linear, decreasing, function of height, $T_m = 1 - 0.5 * y$, which mimics the effects of decreasing melting temperature with decreasing pressure. The initial porosity and permeability were uniform and set to values of 0.01 and 1 and the initial temperature was equal to the melting temperature. Fluid was introduced at the base at the fluidization velocity and temperature 1. Because the melting temperature decreases with height, upward advected fluid will induce melting of the matrix. The effect of latent heat will decrease the temperature where melting occurs and when D is large, as it is in this calculation, the temperature everywhere in the domain will stay close to the melting temperature.

In figure 3 we show the temperature field after 0.16 units of dimensionless time (corresponding to between 5 and 5000 years) with an overlain plot of the fluid velocity. It can be seen that the temperature is close to the melting temperature except that the contours are bowed upward slightly in two regions where the vertical fluid flow is anomalously large. In figure 4 we show a plot of the melting rate at the same time. It can be seen that melting is strongly enhanced in one region of very strong upwelling near x=0.25 and is somewhat enhanced in another region of strong upwelling near x=0.75. In between the spontaneously-formed channels there are regions where solidification is occurring. Freezing occurs between the channels because the downward transport of cold material by the motion of the solid matrix overwhelms the upward transport of hot fluid in these regions which bows the temperature contours downward which is causing the temperature to be less than the melting temperature in these locations. In figure 5 we show the permeability field at the same time. It can be seen that the permeability has been increased by roughly a factor of 7 over its initial value inside the channel at x=0.25. The permeability has been decreased in-between the channels due to compaction and freezing. Because there is a net melting in the simulation domain, a significant degree of compaction has also taken place at the top of the domain which has resulted in a high permeability region there. The formation of the channels occurs because melting increases the porosity of a region which in-turn, increases the permeability. This allows fluid to flow more freely in the channels which increases the transport of heat to these regions which in-turn leads to further melting. A similar mechanism for forming channels has been demonstrated when solute is trans-

ported vertically and there is a net increase in the solute solubility with height (*Aharonov et al.*, 1995, 1997; *Spiegelman et al.*, 2001).

5 Conclusions

We have presented a functioning, 2D, model for flow through a compacting and melting porous layer using COMSOL. The model was formulated using the "primitive" equations for transport in a deformable porous layer. In most previous numerical simulations of compacting porous media (e.g., *Spiegelman et al.*, 2001) potential formulations of the problem are used and the motion of the solid matrix is treated only approximately.

We have shown that once channels are formed, the flow in their vicinity becomes very complex and unfocused on geologically short time scales. We have also shown that channels may be formed spontaneously by pressure-release melting. In future work, it would be interesting to extend the analyses presented here to cylindrical axisymmetric and full three-dimensional geometries. It will also be interesting to investigate processes in magma chambers where porosities are significantly greater and compaction effects are also very significant.

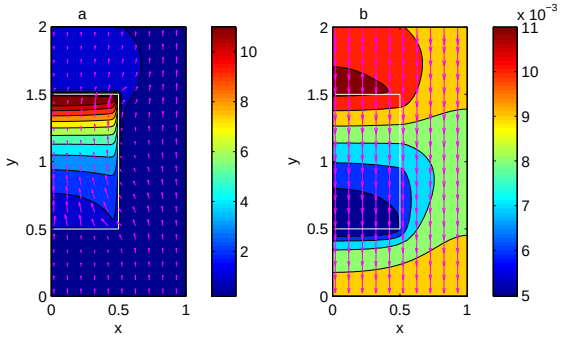

Figure 1: a) The permeability after a short period of time with an overlain arrow plot for the fluid velocity. b) The porosity field after a short periods of time with an overlain arrow plot for the solid matrix velocity.

References

[1] Aharonov, E., J.A. Whitehead, P.B. Kelemen and M Spiegelman, Channeling instability of upwelling melt in the mantle, *Jour. of Geophys. Res.*, *100*, 20 433- 20 450, 1995.

[2] Aharanov, E., M. Spiegelman and P. Kelemen, Three-dimensional flow and reaction in porous media: Implications for the Earth's mantle and sedimentary basins, *102*, 14 821 - 14 833, 1997.

[3] McKenzie, D., The generation and compaction of partially molten rock, *Jour. of Petrology*, *25*, 713-765, 1984.

[4] Phillips, O.M., Flow and Reactions in Permeable Rocks, Cambridge University Press, 1991.

[5] Richter, F., and S. Daly, Dynamical and Chemical Effects of Melting a Heterogeneous Source, *Jour. of Geophysical Research*, *94*, 12,499-12,510, 1989.

[6] Shirley, D.N, Compaction of igneous cumulates, *Jour. of Geology*, *94*, 795-809, 1986.

[7] Spiegelman, M., Flow in deformable porous media. Part 2 Numerical analysis - the relationship between shock waves and solitary waves, *Jour. of Fluid Mech.*, *247*, 39-63, 1993.

[8] Spiegelman, M., P. Kelemen and E. Aharonov, Causes and consequences of flow organization during melt transport: The reaction infiltration instability in compactible media, *Jour. of Geophysical Research*, *106*, 2061-2077, 2001.

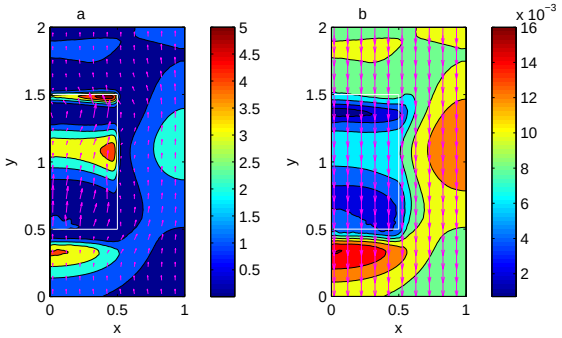

Figure 2: The permeability after a dimensionless time of 0.07 with an overlain arrow plot for the fluid velocity. b) The porosity field after a 0.07 of time with an overlain arrow plot for the solid matrix velocity.

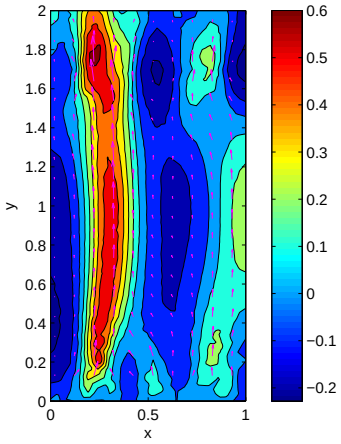

Figure 4: The melting rate after a dimensionless time of 0.16 with an overlain arrow plot for the fluid velocity.

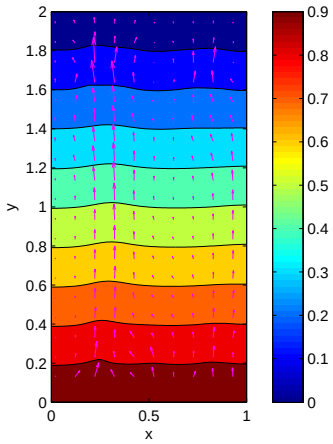

Figure 3: The temperature field after a dimensionless time of 0.16 with an overlain arrow plot for the fluid velocity.

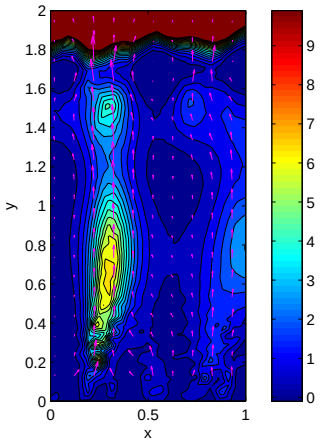

Figure 5: The permeability after a dimensionless time of 0.16 with an overlain arrow plot for the fluid velocity.